Digital imagery analysis of unusual Martian surface features

Mark J. Carlotto

Image processing results in support of ongoing research into the origin of a collection of unusual surface features on Mars are presented. The focus of the investigation is on a mile long feature in the Cydonia region of Mars which resembles a humanoid face that was imaged by Viking orbiter in 1976. While the face has been dismissed as a trick of light and shadow by some, there remains considerable interest in this feature, which others believe was sculpted into the form of a humanoid face, and several nearby polyhedral objects which appear to be spatially aligned with it. Image enhancements of the face show it to be a bisymmetrical object having two eyes, a nose, and a mouth; fine structure in the mouth suggesting teeth are apparent in the enhanced imagery as well as crossed symmetrical lines on the forehead. Facial features are also evident in the underlying 3-D surface which was reconstructed using a single image shape-from-shading technique. Synthetic images derived from the 3-D model by computer graphics techniques suggest that the impression of facial features evident in the original Viking imagery are not a transient phenomenon; i.e., they persist over a wide range of illumination and viewing conditions.

I. Introduction

In July of 1976, the Viking orbiter acquired a strange image of what appeared to be a face staring straight up into space from the surface of Mars. The face was in a region known as Cydonia in the northern hemisphere of Mars, originally selected as a possible landing site for Viking. Officially dismissed at the time as a trick of light and shadow, the face was rediscovered by DiPietro and Molenaar, engineers at the Goddard Space Flight Center, several years later. During the course of their investigation, a second image of the face that had been acquired in slightly different lighting conditions was found. Digital image enhancements of this second image revealed a bisymmetrical object having features suggestive of eyes, a ridgelike nose, and a mouth. Due to the controversial nature of the subject, their results were published independently of the planetary science community.[1]

Initial criticism of their work centered on the human tendency to find faces everywhere; in other words, finding a feature which resembles a humanoid face in isolation on Mars tells us nothing. However, in a subsequent investigation motivated by the work of DiPietro and Molenaar, other nearby objects which seemed to be related to the face were found. In particular, the face appeared to be aligned with a collection of polyhedral objects to the southwest, termed the city, which did not appear to fit the underlying geology of this part of Cydonia. Hoagland, a member of the investigation team, went on to show that solstice alignments between the face and certain objects in the city are satisfied every million years, the last one being about a half a million years ago. Others speculated that the city and face were near the shoreline of an ancient northern sea. Their results were presented at the 1984 Case for Mars Conference.[2] Critics claimed that such objects could not possibly occur on Mars because life, let alone an intelligence capable of creating such things, could not have developed on Mars based on current theories.

In support of more recent work,[3–5] further analysis of the available orbiter imagery using image processing and computer graphics techniques has been performed to obtain the best possible enhancements of these objects and to determine the underlying 3-D structure of the face. Once the 3-D shape has been derived questions such as, what does it look like when viewed in different illumination conditions and from different perspectives?, or does the underlying 3-D structure also resemble a face, or is the impression of a face merely a trick of light and shadow?, can be answered.

The organization of the remainder of this paper is as follows: Sec. II reviews the imagery and data that were made available for the study. Image enhancement results of the face and other nearby objects are presented in Sec. III. Section IV addresses the problem of deriving 3-D information from the available

The author is with Analytic Sciences Corporation, 55 Walkers Brook Drive, Reading, Massachusetts 01867.

Received 1 October 1987.
0003-6935/88/101926-08$02.00/0.

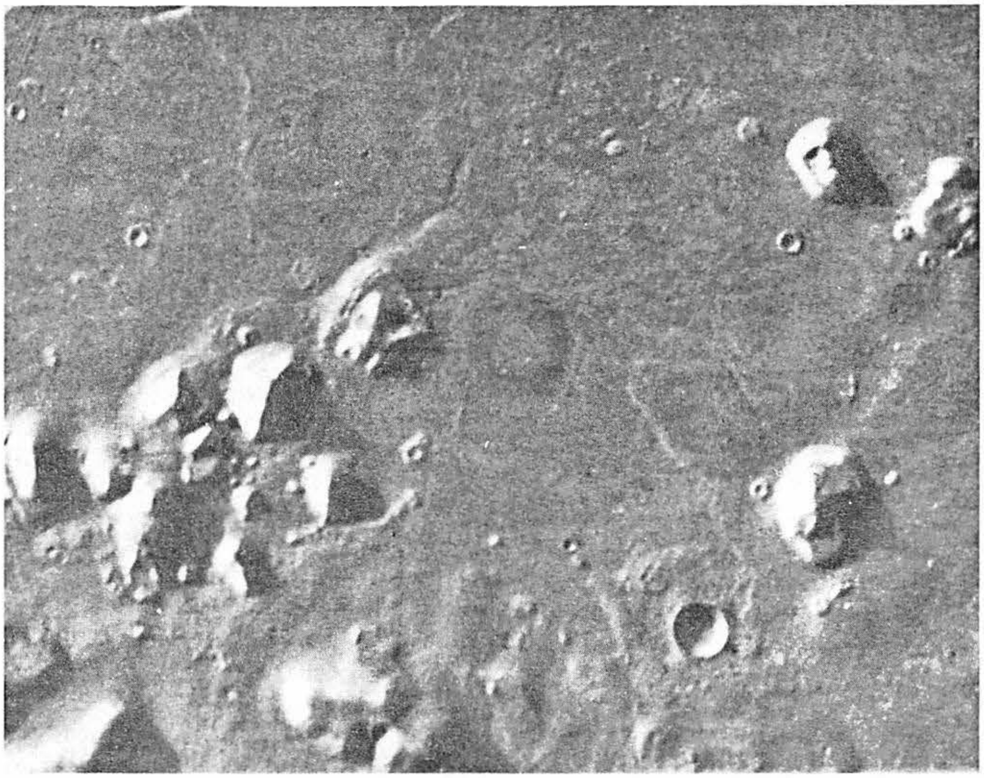

Fig. 1. Contrast-enhanced image of the face and the collection of pyramidal objects to the southwest (the city). The image is ~33.1 × 26.5 km in area and is oriented so that north is up.

imagery. Three-dimensional reconstructions of the face obtained using a single image shape-from-shading technique are presented. The 3-D information is then used to synthesize alternative views in varying illumination conditions and from different perspectives. Results are summarized in Sec. V.

II. Review of the Available Data

The face and other nearby objects are located in the region of Mars known as Cydonia Mensae. The region of interest is in the northern portion of Cydonia Mensae bordering Acidalia Planitia and the northern plains. It is a region containing a variety of flattopped prominences with clifflike walls (mesas) and conical hills or knobs. The geology of this and other parts of Cydonia Mensae are described by Guest and Butterworth.[6] Mesas are 5–10 km wide and are thought to be remnants of cratered plateau material that was subsequently stripped back by erosional processes. Knobs are smaller, ~2 km across, and might be isolated hills with a shallow apron around the base or be on top of mesas. No single mechanism has been suggested for their origin. Geologically, the face would be considered to be a knob.

The face is located at ~40.9°N, 9.45°W. Four images containing the face have been identified and were made available for the study:

35A72—the original photo of the face acquired in the Martian summer, in afternoon light (sun is from the west);

70A13—a second high resolution image containing the face, also in afternoon light, with the sun slightly higher in the sky;

673B56—a lower resolution image of the part of Cydonia Mensae containing the face viewed in afternoon light

753A33—a lower resolution image of the part of Cydonia Mensae containing the face viewed in morning light (sun is from the east)

The above images are referenced in terms of their picture number where 35A72 is the seventy-second image taken in the thirty-fifth orbit by the *A* spacecraft. Frames 35A72 and 70A13 were acquired near periapsis with the spacecraft ~1500 km from the planet; the latter two frames were acquired near apoapses (~33,000 km) when the orbit was shifted for synoptic coverage. Thus, only the first two scenes have sufficient resolution (~50 m/pixel) for our analysis. The second two were useful in that they provided a context for our analysis. Table I summarizes relevant imaging parameters for the two higher resolution images. This information was obtained from the Science Data Block.[7]

Although the planet was viewed in a variety of illumination conditions, only two higher resolution views of the face, both in similar illumination conditions and perspective, were acquired. No higher resolution images of the face in morning light appear to exist. Thus only the features on the left, sunlit side of the face are visible. The following sections describe our efforts to done in computer graphics for producing shaded renditions of surfaces. However, the inverse problem is underdetermined since there are many gradients which will give rise to a particular irradiance.

A relatively simple but elegant method for estimating the gradients is by the method of photometric stereo when two or more images of the scene are available from the same perspective but in different lighting condtions.[11,12] As determined earlier, the two orbiter images are 6.08° apart in view angle; from the Science Data Block one can readily calculate that they are 23.75° apart in sun angle. Thus, the orbiter geometry is better suited for photometric stereo than for stereoscopy. The method of photometric stereo, which was originally developed for relatively low noise industrial machine vision environments, is, unfortunately, very sensitive to noise. Experiments were conducted on both simulated imagery with lighting conditions and noise levels similar to 35A72 and 70A13 and on the actual imagery to assess its usefulness. The resultant gradient fields were noisy and strongly inconsistent; i.e., not readily integratable into elevation surfaces. It was thus concluded that the method of photometric stereo is also not useful for recovering 3-D information from the available imagery.

Finally, we turn to single image shape-from-shading methods. The recovery of shape from a single image is computationally more difficult because we are trying to determine a gradient field with two degrees of freedom from an image which has only one degree of freedom. Various methods have been developed in both the planetary science and the machine vision communities to solve this problem.[11,14] In the planetary community, single image shape-from-shading is known as photoclinometry, a term coined by McCauley in 1965. The method used here was adopted from Strat[15] and Terzopoulis[16] and is based on an iterative multiresolution approach.[17] The height map $z(x,y)$ is computed from a single image $E(x,y)$ in two steps by first estimating the gradients from the image irradiances via the reflectance map and then determining the elevations from the gradients. The iterative approach to shape-from-shading is to be contrasted with those methods which attempt to compute the elevation surface by direct integration of the brightness gradients.[13,14] They, like the method of photometric stereo, are sensitive to image noise and may produce inconsistent gradient fields.

The gradient field (p,q) is estimated by an iterative algorithm which seeks to minimize the integral

$$\iint \{E(x,y) - R[p(x,y),q(x,y)]\}^2 dxdy + \lambda \iint (p_x - q_y)^2 dxdy,$$

where $p_x = \partial p/\partial x$ and $q_y = \partial q/\partial y$. The first term is the difference between the actual and estimated irradiances. The second term forces the gradients to be consistent, i.e., to correspond to a real elevation surface, and also provides a built in immunity to noise. Solution methods for the above equation are discussed in Horn.[11] If p_{ij} and q_{ij} are the sample values of the gradients at the grid point (i,j), the form of the solution is

$$p_{ij}(t+1) = f[p_{ij}(t),q_{ij}(t)] + [E_{ij} - R(p_{ij},q_{ij})]R_p(p_{ij},q_{ij}),$$

$$q_{ij}(t+1) = g[p_{ij}(t),q_{ij}(t)] + [E_{ij} - R(p_{ij},q_{ij})]R_q(p_{ij},q_{ij}),$$

where f and g are linear combinations of the values of p and q around (i,j), $R_p = \partial R/\partial p$, and $R_q = \partial R/\partial q$; the initial conditions are $p_{ij}(0) = 0$ and $q_{ij}(0) = 0$.

In the above algorithm, a penalty term is added to force the gradient field to be consistent. Since consistency is not enforced as a strict constraint, the resultant gradients will be somewhat inconsistent and so cannot be directly integrated into an elevation surface. Therefore, the elevation map $z(x,y)$ is computed by another iterative algorithm which minimizes the integral:

$$\min \iint [(z_x - p)^2 + (z_y - q)^2]dxdy,$$

where $z_x = \partial z/\partial x$ and $z_y = \partial z/\partial y$.

The algorithm used here assumes a flat background as a boundary condition. Other shape-from-shading algorithms use different boundary conditions such as occluding boundaries, or in photoclinometry, planetary limbs. The algorithm also forces the reconstructed surface to follow the grazing rays of the sun in shadowed areas. This provides an implicit boundary condition that in turn forces the lengths of shadows to agree with the heights of the objects casting the shadows.

C. Imaging Model

Before applying the shape-from-shading algorithm to the imagery, the salient characteristics of the atmosphere, the imaged surface, and the illumination must be considered. In addition to the orthographic imaging assumption stated earlier, five additional assumptions are made:

(1) the atmosphere is a horizontally homogeneous medium;

(2) the surface material compositon is homogeneous and the albedo is constant within the region of interest;

(3) the surface can be modeled as a Lambertian reflector;

(4) the sun can be approximated as a point source and the sky by a uniform hemispherical source; and

(5) some portion of the region of interest directly faces the sun, some portion is in shadow, and the area surrounding the face is flat.

The first assumption allows us to reduce a 3-D problem to a 1-D problem.[18] Assumption two is based on observations by Wildey[13] that the winds tend to redeposit surface materials in a uniform fashion so the albedo and scattering properties can be treated as approximately constant over small areas. Assumption three was made in lieu of specific knowledge about the composition of surface materials in Cydonia. The paucity of imagery over the region of interest precluded an empirical estimation of the reflectance map (photometric function) via a Minneart or Lommel-Seeliger fit, for example. The results presented in the next section show that, to a first order, the Lambertian is a good model over the region of interest. The point source and hemispherical sky assumptions are made to

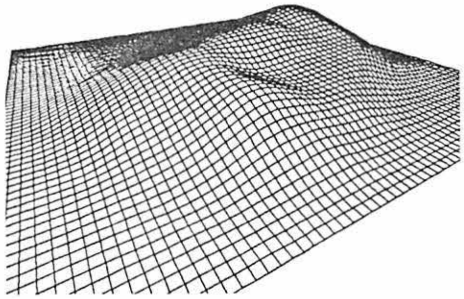

Fig. 5. Isometric plot of the 3-D reconstruction obtained using the single image shape-from-shading algorithm on 70A13. A similar result was obtained for 35A72.

simplify the reflectance map. To check the validity of the point source assumption, the sun was modeled as an extended source (0.34° at Mars) and found to have a negligible effect on the surface reconstruction. The hemispherical sky term is used to model ambient light (more on this below). Finally, the last assumption allows image intensities to be converted into normalized reflectances between zero and one for shape-from-shading and supplies the needed boundary condition.

The resultant image formation model (adapted from Sjoberg[18]) is given by

$$L(x,y) = (\rho/\pi)T_u(z)\{E_0T_d(z)R[p(x,y),q(x,y)] + E_s(z)R_a[p(x,y),q(x,y)]\} + L_p(z),$$

where $L(x,y)$ is the radiance, ρ is the albedo, $T_u(z)$ is the vertical atmospheric transmittance from altitude z up to the spacecraft, E_0 is the extraterrestrial solar irradiance, $T_d(z)$ is the path transmittance from the sun to altitude z, $R(p,q)$ is the reflectance map for a Lambertian scatterer illuminated by a point source, $E_s(z)$ is the sky irradiance at altitude z, $R_a(p,q)$ is the reflectance map for a Lambertian scatterer under a uniform hemispherical source, and $L_p(z)$ is the path radiance between the spacecraft and the surface at altitude z. Since the field of view is small and the variation in altitude is small relative to the depth of the atmosphere within the field of view, we treat $T_u(z)$, $T_d(z)$, $E_s(z)$, and $L_p(z)$ as constants. The low digital counts in the shadows suggest that $E_0T_d \gg E_s$ and that the contribution of the L_p term on the right side is small (but not zero). However, given the limited dynamic range of the data and the relatively high noise level, we shall assume that it is negligible and, for the present, shall concern ourselves with the portion of the face that is directly illuminated by the sun.

Assuming an orthographic imaging model, the previous equation can be simplified as

$$E(x,y) = k_1R[p(x,y),q(x,y)] + k_2,$$

where k_1 and k_2 are constants. Assuming a linear relationship between the image irradiance $E(x,y)$ and the digital image intensity data $I(x,y)$, image intensities and reflectances can be related by

$$I(x,y) = (I_{\max} - I_{\min})R[p(x,y),q(x,y)] + I_{\min}.$$

$I_{\max}$ is assumed to correspond to areas that face the sun ($R = 1$) and $I_{\min}$ is assumed to correspond to areas in shadow ($R = 0$). Finally, the reflectance map for a Lambertian surface illuminated by a point source at (p_0,q_0) is given by

$$R(p,q) = \frac{1 + pp_0 + qq_0}{(1 + p^2 + q^2)^{1/2}(1 + p_0^2 + q_0^2)^{1/2}},$$

where $p_0 = \tan\phi_0 \cos(90 + \theta_0)$ and $q_0 = \tan\phi_0 \sin(90 + \theta_0)$. The angle ϕ is measured relative from the zenith and the azimuth angle θ is measured clockwise from north. Values of p_0 and q_0 for 35A72 and 70A13 are derived from the ephemeris data in Table I.

D. Results

Reconstructions of the face were computed from 35A72 and 70A13 using the single image shape-from-shading algorithm. An isometric plot of the elevation map computed from 70A13 is shown in Fig. 5. The view is from the northwest, i.e., above and to the left of the face. An almost identical result was obtained from 35A72. Both results clearly show evidence of facial features in the underlying topography. The reconstructed shape of the face appears somewhat smoother than one would expect from looking at the imagery since the area is rather small to begin with (64 × 64 pixels total), derivatives are estimated locally within 3 × 3 windows, and the presence of the consistency constraint in the iterative formulation has the effect of trading off detail for reduced noise.

To check the validity of the results, synthetic images were computed from the gradient fields of the reconstructed surfaces and compared to the original data. Figures 6(a) and (b) are the original images from 35A72 and 70A13. Figures 6(c) and (d) are the synthetic images obtained by illuminating the 3-D surface reconstructed from 35A72 with the light source at positions corresponding to 35A72 and 70A13, respectively. Figures 6(e) and (f) are the synthetic images obtained by illuminating the 3-D surface computed from 70A13 with the light source at positions corresponding to 35A72 and 70A13, respectively. The close agreement between (a), (c), and (e), and (b), (d), and (f) suggests that the Lambertian model assumption is adequate given the quality of the data.

Synthetic images of how the 3-D surface might appear in different illumination conditions are shown in Fig. 7. The images in the figure were generated by substituting the gradients estimated by the shape-from-shading algorithm into the reflectance map equation for different light source positions. The facial features evident in the original orbiter photographs are also present in different illumination conditions. Under simulated morning light, the left side of the face is dark and the left eye is bright while in afternoon light the situation is reversed.

To simulate the appearance of the face from different perspectives, the image of the face from 35A72 was projected onto the elevation map computed above and reprojected using a computer graphics rendering system. The renderer can generate perspective views of 3-D scenes for arbitrary camera positions. In this case

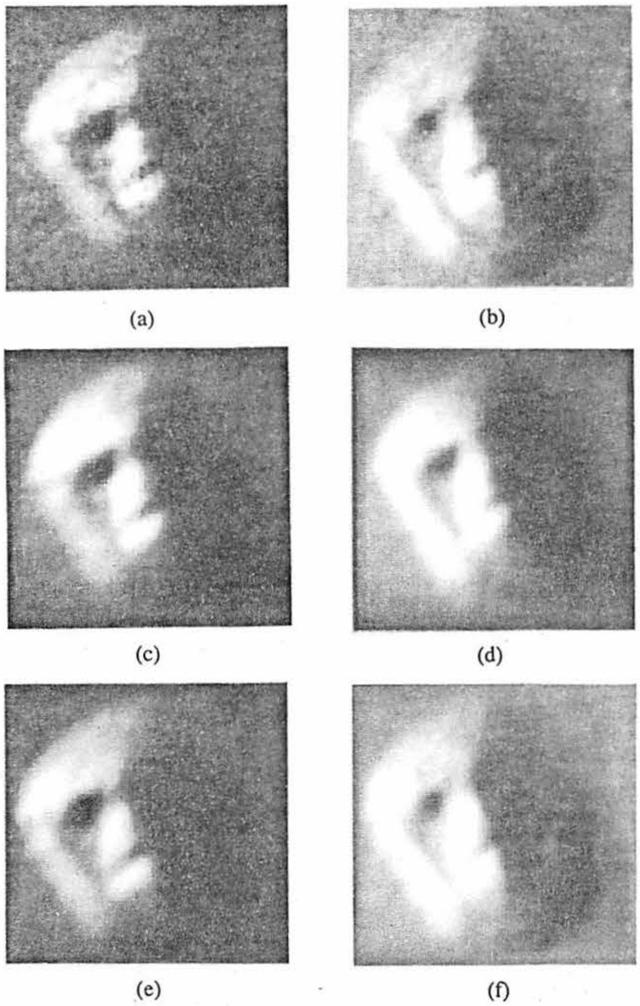

Fig. 6. Cross-check of single image shape-from-shading results: Original images of (a) 35A72 and (b) 70A13. Synthetic images of the 3-D surface estimated from 35A72 and viewed in lighting conditions of (c) 35A72 and (d) 70A13. Synthetic images of the 3-D surface estimated from 70A13 and viewed in lighting conditions of (e) 35A72 and (f) 70A13.

the 3-D scene was the image in 35A72 projected onto the 3-D surface computed by the shape-from-shading algorithm. Simulated images for different positions around the face are shown in Fig. 8. Again, the facial features evident in the downlooking view of the orbiter photography are also present when the object is viewed from radically different perspectives. Such is not the case in more familiar terrestrial analogs such as New Hampshire's Old Man of the Mountain, for example.

Finally measurements of the peak height, length, width, and maximum slope of the feature were made for both 3-D surfaces. The peak height was corroborated by measuring the length of the shadows. In general, the results presented in Table II show good agreement between the two images.

V. Summary and Conclusions

Digital image enhancements of a mile long feature resembling a humanoid face and other nearby objects in the Cydonia region of Mars were performed, the 3-D

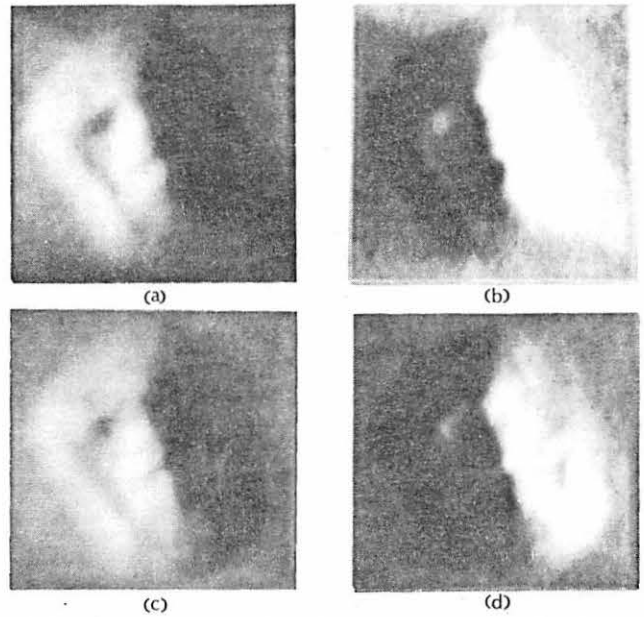

Fig. 7. Synthetic images of the face as it might appear in different illumination conditions. Images (a) and (c) were obtained by illuminating the 3-D surfaces computed from 35A72 and 70A13 under simulated afternoon light. Images (b) and (d) are the corresponding views under simulated morning light.

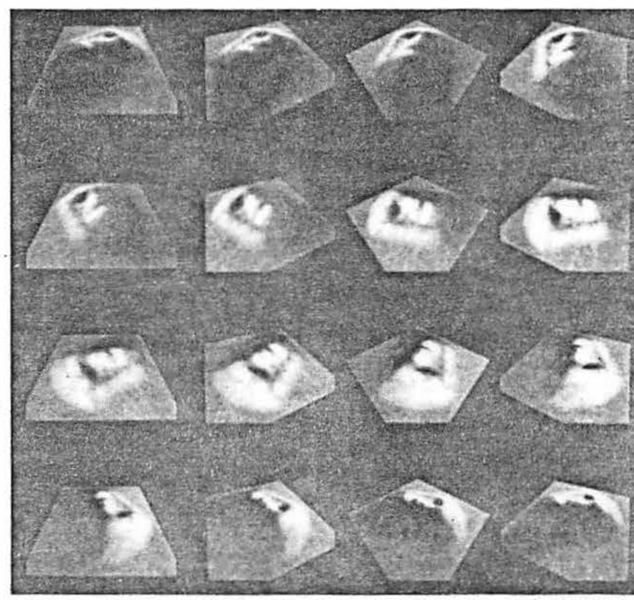

Fig. 8. Perspective views of the face generated by projecting the image of 35A72 onto its 3-D surface. The views were generated for simulated camera positions around the face.

Table II. Measurements of the Face Derived from Viking Orbiter Imagery

Measurement	35A72	70A13	Combined
Peak height	430 m	395 m	412.5 ± 17.5 (4.2%)
Length	2.62 km	2.46 km	2.54 ± 0.08 (3.1%)
Width	2.06 km	2.03 km	2.045 ± 0.015 (0.7%)
Maximum slope	44.83°	33.18°	39.01 ± 5.82 (15%)

structure of the face was derived using a single image shape-from-shading algorithm, and synthetic views were then generated using computer graphics techniques. The 3-D analysis was performed because there is a lack of high resolution images of this area viewed in conditions other than in afternoon light and from directly overhead. The intent was to create synthetic views of the face to determine if the visual impression of a face persists over a wide range of lighting conditions and perspectives.

The image enhancement results indicate that a second eye socket may be present on the right, shadowed side of the face; fine structure in the mouth suggesting teeth are apparent in the enhanced imagery as well as crossed symmetrical lines on the forehead. The results of the 3-D analysis show that the impression of facial features is not a transient phenomenon. Facial features are evident in the underlying topography and are shown to induce the visual impression of a face over a wide range of illumination conditions and perspectives.

It is the author's belief that, although the Viking data are not of sufficient resolution to permit the identification of possible mechanisms of origin for these objects, the results to date suggest that they may not be natural. At the very least, these enigmatic objects deserve further scrutiny by future Mars probes such as the 1988 Soviet Phobos mission or the U.S. Mars Observer.

References

1. V. DiPietro and G. Molenaar, *Unusual Martian Surface Features* (Mars Research, Glenn Dale, MD, 1982).
2. R. Hoagland, "Preliminary Report of the Independent Mars Investigation Team: New Evidence of Prior Habitation?," presented at Case for Mars II Conference, Boulder, CO (July 1984).
3. R. Pozos, *The Face on Mars: Evidence for a Lost Civilization?* (Chicago Review Press, IL, 1986).
4. R. Grossinger, "The Face on Mars: an Interview with Richard Hoagland," in *Planetary Mysteries* (North Atlantic Books, Berkeley, CA, 1986).
5. R. Hoagland, *The Monuments of Mars* (North Atlantic Books, Berkeley, CA, 1987).
6. J. E. Guest and P. S. Butterworth, "Geological Observations in the Cydonia Region of Mars from Viking," J. Geophys. Res. **82**, 4111 (1977).
7. M. Carr, *The Surface of Mars* (Yale U.P., New Haven, 1981).
8. V. Tom, "Adaptive Filter Techniques for Digital Image Enhancement," Proc. Soc. Photo-Opt. Instrum. Eng. **528**, 121 (1985).
9. E. Grimson, *From Images to Surfaces* (MIT Press, Cambridge, MA, 1981).
10. C. Sloma, Ed., *Manual of Photogrammetry* (American Society of Photogrammetry, Falls Church, VA, 1980).
11. B. Horn, *Robot Vision* (MIT Press, Cambridge, MA, 1986).
12. R. J. Woodham, "Photometric Method for Determining Surface Orientation from Multiple Images," Opt. Eng. **19**, 139 (1980).
13. L. Wildey, "Generalized Photoclinometry for Mariner 9," Icarus **25**, 613 (1975).
14. T. Rindfleisch, "Photometric Method for Lunar Topography," Photogramm. Eng. **32**, 262 (1966).
15. T. M. Strat, "A Numerical Method for Shape from Shading from a Single Image," S.M. Thesis, Department of Electrical Engineering & Computer Science, MIT, Cambridge, MA (Jan. 1979).
16. D. Terzopoulis, "Computing Visible-Surface Representations," Memo AIM-800, MIT Artificial Intelligence Laboratory, Cambridge, MA (Mar. 1985).
17. P. Van Hove and M. Carlotto, "An Iterative Multi-Resolution Shape-from-Shading Algorithm and Its Application to Planetary Mapping," *International Geoscience and Remote Sensing Symposium*, Zurich (Sept. 1986).
18. R. W. Sjoberg, "Atmospheric Effects in Satellite Imaging of Mountainous Terrain," TR-688, MIT Artificial Intelligence Laboratory, Cambridge, MA (Sept. 1982).

The eighth International Photopolymer Conference: Principles, Processes and materials , will be held at the Nevele Country Club, Ellenville, New York, Oct. 31-Nov. 2, 1988. Sponsored by the Mid-Hudson Section, Society of Plastics Engineers.

The conference will cover Optical, Electron Beam, and X-Ray lithographic materials and processes.

Contact P.R. Shah, C/O IBM Corp., D/959-40E, RT 52, Hopewell Junction, N.Y. 12533. (TEL: 914-894-3230)